

## EBW Simulations in an Experimental Context

J. Urban<sup>1</sup>, J. Preinhaelter<sup>1</sup>, S.J. Diem<sup>2</sup>, H.P. Laqua<sup>3</sup>, P. Pavlo<sup>1</sup>, V. Shevchenko<sup>4</sup>, G. Taylor<sup>5</sup>,  
G. Vahala<sup>6</sup>, L. Vahala<sup>7</sup> and M. Valović<sup>4</sup>

<sup>1</sup> EURATOM/IPP.CR Association, Institute of Plasma Physics, 182 00 Prague, Czech Rep.

<sup>2</sup> Oak Ridge National Laboratory, Oak Ridge, TN 37831, USA

<sup>3</sup> Max-Planck-Institut für Plasmaphysik, EURATOM Association Greifswald, Germany

<sup>4</sup> EURATOM/UKAEA Fusion Association, Culham Science Centre, Abingdon, UK

<sup>5</sup> Princeton Plasma Physics Laboratory, Princeton, New Jersey 08543, USA

<sup>6</sup> College of William & Mary, Williamsburg, VA 23185, USA

<sup>7</sup> Old Dominion University, Norfolk, VA 23529, USA

(Received: 1 September 2008 / Accepted: 16 February 2009)

In the past several years we have been developing simulation techniques for electron Bernstein wave (EBW) physics in toroidal fusion devices. EBW simulations are rather difficult for several reasons. EBWs are electrostatic waves, whose propagation is strongly affected by the plasma parameters. EBWs cannot propagate in a vacuum and must be coupled to X- and/or O-modes. The conversion efficiency must be in general computed numerically by a full-wave solver.

Details of our code AMR are described. This includes electrostatic ray-tracing, EBW root finder and 1D full-wave adaptive finite elements solver of the EBW-X-O mode conversion. The plasma configuration is handled by independent modules and typically obtained from experimental results. A Python driver script handles user configuration files and is able to parallelize the simulation.

We describe applications of AMR to support various experiments. It is used to interpret EBW emission from the spherical tokamaks MAST and NSTX, to confirm the resonant EBW heating on the WEGA stellarator, to model its new 28 GHz system and to predict the applicability of the designated EBW emission radiometer for COMPASS.

Keywords: plasma, fusion, tokamak, stellarator, electron Bernstein wave, simulation, full-wave, ray-tracing.

### 1. Introduction

Electron Bernstein waves (EBWs) [1] are electrostatic modes with frequencies in the electron cyclotron range. They have no upper density limits, which makes them a viable option for applications in overdense ( $\omega_{pe}^2 \gg \omega_{ce}^2$ , where  $\omega_{pe}$  is the electron plasma frequency and  $\omega_{ce}$  the electron cyclotron frequency) fusion plasmas. Spherical tokamaks and stellarators operate routinely in overdense regimes. EBWs can be used for heating and current drive as well as for various diagnostics.

This paper is focused on computer simulations of EBWs, with particular reference to the experiments. EBW simulations are rather difficult for several reasons. EBWs are electrostatic waves, whose propagation in a plasma are quite strongly affected by the plasma configuration as compared to other electron cyclotron waves. Moreover, EBWs cannot propagate in a vacuum and thus must be

coupled to X and O modes at the upper hybrid resonance region (UHR). The conversion efficiency at the UHR must be in general computed numerically by a full-wave solver.

We will describe the simulation code AMR (Antenna – Mode conversion – Ray-tracing), which includes a full-wave –conversion efficiency solver, an electrostatic non-relativistic ray-tracing solver, modules for reading and interpreting plasma parameters and a Python driver script. Important recent results for the spherical tokamaks MAST and NSTX, the stellarator WEGA and the reinstalled COMPASS tokamak [2] are presented.

### 2. Electron Bernstein Wave Simulation

We now describe the numerical techniques involved in the simulation code AMR. Many particular details have been already published; therefore, we present only an overall description with emphasis on new features. We note that the name AMR is used here for the first time for

our code.

The O-X-EBW mode conversion process [3, 4] is treated in plain stratified plasma slab geometry, thus neglecting 2D effects. Particularly for off-axis launch, the O-X-EBW and EBW-X-O conversions are asymmetric in 2D [5]. The cold plasma model is used, which permits the calculating of any electron cyclotron harmonic in the same manner. The corresponding set of ordinary differential equations (ODEs) is solved with an adaptive finite elements method (FEM) [6, 7]. The FEM is generally more complex when compared to the standard ODE solvers (e.g. Runge-Kutta). It is, however, very well suited [8, 9] for the conversion efficiency problem with almost singular, stiff equations with spurious, exponentially growing solutions. If the reverse EBW-X-O mode conversion is considered, e.g. in electron Bernstein wave emission (EBE) simulations, general symmetries imply the reciprocity of these processes [10, 11] and thus the conversion efficiencies are equal.

The ray-tracing part of our code [12] uses a non-relativistic, electrostatic hot plasma dispersion relation. This approximation provides the simplest, yet fastest way to treat EBWs. Relativistic corrections become prominent at electron temperatures  $T_e \gtrsim 1$  keV [13] and we plan to incorporate them in the near future. Relativistic dispersion is, however, quite complicated for EBWs [14] and, consequently, slower to evaluate. The radiative transfer equation is solved, along the standard ray equations [15], in the temporal domain with the focusing terms neglected [16]:  $dP/dt = \alpha - \eta P$ , where  $P$  is the ray power,  $\alpha$  is the absorption coefficient and  $\eta$  the emission coefficient. The receiving (transmitting) antenna beam is then represented by a set of rays, each having their own corresponding intensity. To obtain the value of a particular quantity for the whole beam, the results from the individual rays are appropriately weighted (i.e. multiplied by the intensity factor etc.) and integrated over the beam waist.

Magnetic configuration and electron density and temperature profiles must be provided for the calculations described above. The magnetic configuration in a tokamak is axisymmetric and can be described by two functions: the poloidal magnetic flux function  $\psi(R, Z)$  and the toroidal magnetic flux function  $F(\psi)$ , which satisfy the Grad-Shafranov equation. The magnetic field is determined from  $B_r = -R^{-1} \partial \psi / \partial Z$ ,  $B_\phi = F/R$  and  $B_z = R^{-1} \partial \psi / \partial R$ . Here and in the following, we use the typical cylindrical coordinate system  $(R, \phi, Z)$  with  $\phi$  the toroidal angle around torus and  $Z=0$  the torus midplane (the equatorial plane). The magnetic field and its first derivatives are necessary for EBW simulations. Therefore the second derivatives of  $\psi$  and the first derivative of  $F$  are needed. For that reason, high order splines are used to interpolate  $\psi(R, Z)$  and  $F(\psi)$ .

Stellarator magnetic configurations are more complex as they have a 3D structure. A numerical library, developed in IPP Greifswald, which is also used in the TRAVIS code [17], is incorporated in our code to operate these 3D equilibria. It imports Boozer coordinates data, interpolates them and via its Fortran interface provides all required equilibrium quantities, particularly the magnetic field vector and its derivatives, the flux label etc. 3D equilibria can be important for tokamaks as well, when taking toroidal field ripple into account.

Electron density ( $n_e$ ) and temperature ( $T_e$ ), along with their derivatives, are needed at all locations inside the computational domain. We assume that  $n_e$  and  $T_e$  are constant on a flux surface, i.e. they are functions of  $\psi$ . This is of course not true outside the separatrix, where the flux surfaces are not closed. However, as we need the profiles there as well, we nevertheless assume that  $n_e$  and  $T_e$  are functions of  $\psi$ . This is adequate as long as we are close to the equatorial plane, where EBWs are launched (detected) and where the profiles are measured.  $n_e(\psi)$  and  $T_e(\psi)$  thus provide a complete 3D plasma model necessary for our simulations. Various B-spline routines from IMSL or NAG Fortran libraries are employed to interpolate the provided datasets. The choice of the interpolation method can be very important. The input profiles can be either experimental data or analytical formulas. Experimental data are preferred against analytical formulas to construct our model to remain as close to reality as possible. There are a variety of diagnostics measuring these profiles, with Thomson scattering (TS) usually operating routinely on larger tokamaks. TS can detect both electron density and temperature. Experimental data are naturally polluted with errors. The largest errors are typically located in the scrape-off layer, outside the last closed flux surface (LCFS). Therefore, the profiles must be processed first and any erroneous data points excluded. Also, data points are sometimes missing in the scrape-off layer. In this case, we use an exponentially decaying extrapolation. The density profile must be assumed monotonic in the conversion efficiency calculation domain, i.e. typically from the edge to several centimeters inside the separatrix (or better to the plasma cut-off, where  $\omega^2 = \omega_{pe}^2$ ).

The whole AMR code is divided into well separated modules. There is a conversion efficiency module and a ray-tracing module, which is closely connected to a module that seeks the ray-tracing initial conditions, i.e. the  $k_\perp$  roots of the dispersion relation. Equilibrium functions are inside a single module, while density and temperature functions are in a different module. There are various supporting modules, for, e.g., vector operations or ray/beam operations. The final integration is in fact a separate program, although it shares a lot of the code base. The code is implemented in Fortran 90/95, which is frequently used in the plasma physics community and

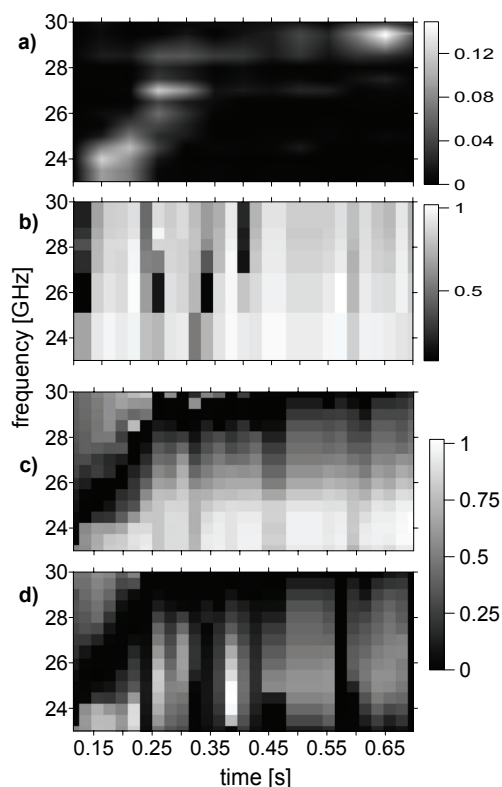


Fig.1 a) Experimental  $T_{\text{rad}}$  [keV], b) simulated EBW-X-O conversion efficiency, c) simulated  $T_{\text{rad}}$  without collisions, d) simulated  $T_{\text{rad}}$  including collisions. NSTX shot 120910.

well suited for numerical simulations. Modern and powerful compilers are widely available.

The driver script, written in Python, serves several purposes. It reads user inputs from a synoptic text file and, if necessary, experimental data from a database. From these data it creates input files for the Fortran code. Our simulations can be straightforwardly parallelized as the calculation for each ray is entirely independent of the other rays except for the final integration. The Python script can, if run on a cluster, divide the whole calculation into smaller jobs, distribute them over the available processors and collect the results. Thus the performance of the code increases practically linearly with the number of processors. Finally, the script invokes the integration code. This makes the user interface very friendly, as the user edits two configuration files (from which one stores the antenna configuration) and executes a single command.

Recently, we predicted EBW current drive for the WEGA stellarator. This prediction was based on ray-tracing calculations, which showed that the symmetric  $N_{\parallel}$  spectrum of the double slot antenna becomes highly asymmetric. Almost all rays, which start typically with  $N_{\parallel}$  around  $\pm 0.7$ , are absorbed with large  $|N_{\parallel}|$  of the same sign. We first modulate our simulation by calculating “directional” power absorption profiles,

where the absorbed power is multiplied by the sign of the driven current. Assuming Fish-Boozer current drive mechanism (since the trapped particle population is unimportant), this sign is opposite to the parallel resonant velocity  $v_{\parallel}^{\text{res}} = (\omega - n\omega_{ce})/k_{\parallel}$ , where  $n$  is the harmonic number. This is, of course, a very basic estimate, which cannot predict the current drive efficiency. A better estimate, suggested by Hansen *et al.* [18], has been added recently. Implementation of the CURBA routine, based on [19], and coupling to the LUKE Fokker-Planck code [20] are envisaged.

### 3. NSTX and MAST results

Various results were obtained with our code for EBE experiments on NSTX [21] and MAST [22] spherical tokamaks. For NSTX, the simulated temporal evolution of the first harmonic L-mode emission was in an excellent agreement with measurements [23]; antenna aiming or equilibrium reconstruction studies were also performed [24]. The wide frequency spectra detectable on MAST allowed, for example, edge profiles reconstructions or antenna aiming and polarization effects to be studied [25].

There have been numerous NSTX H-mode discharges in recent years, for which EBE radiation temperatures were extremely low. Typically, the radiation temperature dropped significantly after the L- to H-mode transition. Conversion efficiency calculations predicted almost 100 % conversion for these cases and could not explain this behavior. Only ray-tracing calculations with collisional absorption of EBWs predicted a large decrease in the emission intensity. EBWs can be collisionally absorbed at the edge, where the electron temperature is low and the electron-ion collision frequency can be  $\nu_{ei} \approx 10^{-4} \omega$ . As EBWs propagate from the dense plasma, they reflect near the upper hybrid resonance (UHR), where their group velocity is almost reversed and tends to be very low. During the propagation back (towards higher density), they convert to the X-mode. The low group velocity and the resulting relatively long time of propagation through the high collisional region make EBWs very sensitive to collisional damping, in contrast to the propagation of the transversal X- and O-modes. The UHR of the 1<sup>st</sup> and 2<sup>nd</sup> harmonic EBWs is frequently located in the scrape-off layer, where the electron temperature is very low, which intensifies the collisional damping. Various dynamical processes occurring in the scrape-off layer may lead to multiple UHRs, i.e. non-monotonic electron density profiles, as repeatedly detected by the TS system. These UHR multiplicities may cause significantly lower conversion efficiencies. It cannot, however, be modeled by our conversion efficiency solver, which, because of the cold plasma model, cannot handle multiple UHRs.

The detected EBE radiation temperature ( $T_{\text{rad}}$ )

spectrum along with the simulation results for NSTX shot 120910 is shown in Fig. 1. The apparent blocking of the EBE from approx. 0.3 s is partially present in the simulation results which include the collisional damping. The simulations are sensitive to edge plasma profiles which, unfortunately, are not measured very accurately in the scrape-off layer. These inaccuracies could be responsible for the disagreements. The sensitivity of the EBE to edge plasma conditions was recently confirmed experimentally [26]. With the help of the lithium evaporator, edge conditions were changed on similar NSTX discharges. Particularly the electron temperature at the UHR was varied. The EBW radiation temperature significantly increased with the electron temperature at the UHR.

#### 4. Simulations for the WEGA stellarator

Overdense plasmas in the WEGA stellarator are well suited for studying EBWs [27]. WEGA is a medium-sized classical  $\ell=2$ ,  $m=5$  stellarator, with major radius of 72 cm and maximum minor plasma radius of 11.5 cm. We employ the library (described above) operating on VMEC [28] outputs for the equilibrium. Analytically fitted probe measurement data are used for density and temperature profiles. WEGA discharges are sustained with a 2.45 GHz heating. The magnetic field  $B_0$  is varied in the range  $B_0/B_{\text{res}} = 0.6 - 0.9$ , where  $B_{\text{res}} = \omega m_e / e \cong 0.0875$  T is the resonant magnetic field. The plasma is highly overdense with peak electron plasma frequency  $f_{pe} \gg 2.45$  GHz. Characteristic of WEGA is a fast electron population, generated by the 2.45 GHz heating, with  $T_e^{\text{fast}} \cong 300$  eV and densities around 10 – 20 % of the total electron density. The bulk electron temperature  $T_e^{\text{bulk}} \lesssim 10$  eV. We treat the fast electrons as an independent plasma component with a Gaussian distribution. In this case, the contributions from the two components can be simply summed in the electrostatic dispersion relation.

In the beginning, the resonant EBW absorption of the 2.45 GHz heating was verified by our simulations [29]. At the same time, EBW current drive was predicted and later on experimentally observed [30]. We presently test the Hansen formula to obtain the values of the current drive efficiency and the total driven current. These results are compared to experimental data. The working gas in WEGA is argon. The current drive efficiency is in this case significantly decreased by inelastic collisions, i.e. electron impact ionizations and excitations with argon ions and neutrals. These collisions are quite frequent as most of the current is carried by the fast component, whose energy yields the largest cross sections for these collisions.

A new 28 GHz ECRH system is starting to operate on WEGA. This frequency is appropriate for second harmonic heating with the central toroidal magnetic field  $B_0 \cong 0.5$  T. If the electron density exceeds  $\sim 10^{19}$  m<sup>-3</sup>,

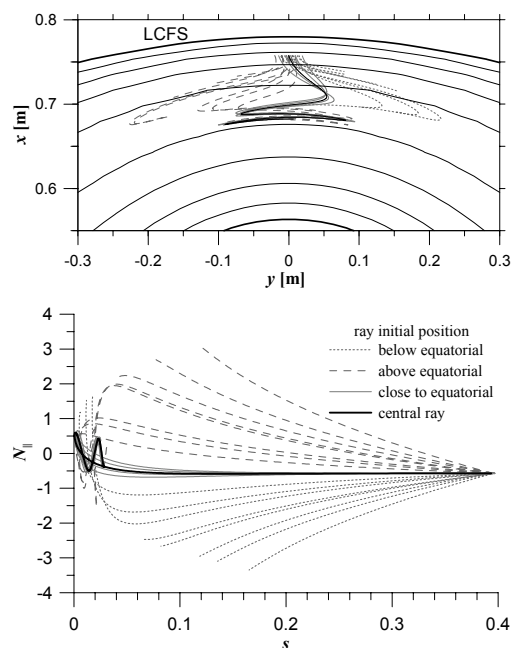


Fig.2 Top – 28 GHz ray trajectories in WEGA toroidal cross section. Bottom –  $N_{\parallel}$  evolution of these rays versus the flux label  $s$  (0 on the magnetic axis, 1 on the separatrix).

the plasma becomes overdense for X- and O-modes. These can, however, convert to EBWs. For this reason, the antenna is able to launch the waves obliquely. Our calculations show that the O-X-EBW conversion efficiency can reach 100 % with optimum aiming and polarization. Ray-tracing shows (see Fig. 2) that EBW rays propagate to the magnetic axis vicinity, where they are efficiently absorbed on the second electron cyclotron harmonic. The  $N_{\parallel}$  spectrum is symmetric in this case and therefore no current is driven. There is also much lower  $|N_{\parallel}|$  growth, contrary to the 2.45 GHz case, and hence the Doppler shift is much weaker. The 28 GHz system appears to be an efficient heating system with centralized power deposition and no current drive.

#### 4. COMPASS predictions

COMPASS is a mid-sized, conventional aspect ratio tokamak with ITER-like plasma shape, which was moved from UKAEA Culham to Prague [2]. Numerous upgrades are planned, for example neutral beam injection heating and advanced diagnostics. EBWs will be extensively studied by detecting EBE with a steerable 16-channel radiometer [31]. The frequency range will be 26 – 40 GHz for first harmonic detection at  $B_0 = 1.2$  T and, with a different front-end, 60 – 90 GHz for the second harmonic or the first harmonic at higher magnetic fields. The higher frequency range can be also used for standard electron cyclotron emission detection.

We were able to obtain optimum antenna angles for the EBE detection. These angles are predominantly

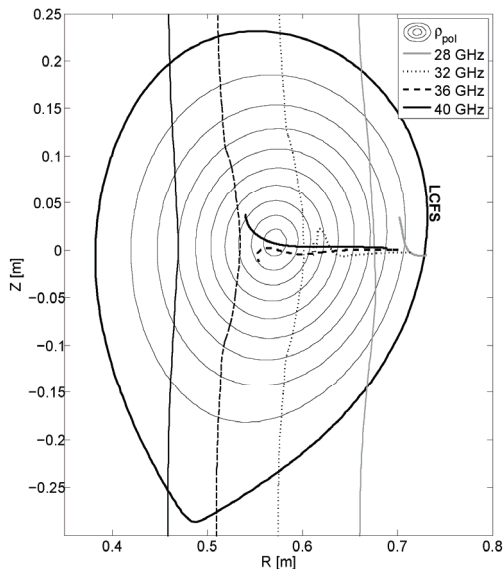


Fig.3 Central ray trajectories for various frequencies and their respective electron cyclotron resonances in the poloidal cross-section of COMPASS.

determined by the angular dependence of the conversion efficiency. In Fig. 3, we plot the ray trajectories of the central rays with frequencies from the first harmonic range. First we see that this range covers approximately 3/4 of the COMPASS electron cyclotron first harmonic range. The coverage of the EBE system is determined by the location where the rays are emitted, i.e. at the ends of the ray curves in Fig. 3. The 34 – 36 GHz emission originates very close to the magnetic axis and may be utilized for central electron temperature detection. Higher frequencies do not start notably further because of a larger Doppler shift.

## 5. Summary

The code AMR can be used for a range of EBW simulations. In particular, simulations of emission from spherical tokamaks, heating on a stellarator or EBE system applicability were successfully performed. Moreover, additional enhancements are foreseen, such as relativistic ray-tracing and sophisticated current drive calculations. The code is supported by a user-friendly interface and is capable of parallel calculations on multiple processors. These properties make AMR an excellent EBW simulation tool.

## Acknowledgement

Partly supported by the Grant No. 202/08/0419 of the Czech Science Foundation, by EURATOM, by the U.S. Department of Energy and by INTAS ref. no. 05-1000008-8046.

- [1] I. B. Bernstein, *Physical Review* **109**, 10 (1958).
- [2] R. Pánek *et al.*, *Czech. J. Phys.* **56**, B125 (2006).
- [3] J. Preinhaelter, and V. Kopecký, *J. Plas. Phys.* **10**, 1 (1973).

- [4] J. Preinhaelter, *Czech. J. Phys.* **25**, 39 (1975).
- [5] A. Y. Popov, *Plasma Physics and Controlled Fusion* **49**, 1599 (2007).
- [6] J. Urban, and J. Preinhaelter, *Czech. J. Phys.* **54**, C109 (2004).
- [7] J. Urban, and J. Preinhaelter, *J. Plas. Phys.* **72**, 1041 (2006).
- [8] K. Appert *et al.*, *Computer Physics Communications* **40**, 73 (1986).
- [9] M. A. Irzak, and O. N. Shcherbinin, *Nuclear Fusion* **35**, 1341 (1995).
- [10] A. Bers, and A. K. Ram, *Physics Letters A* **301**, 442 (2002).
- [11] A. D. Piliya, and A. Y. Popov, *Plasma Physics and Controlled Fusion* **44**, 467 (2002).
- [12] P. Pavlo, L. Krlin, and Z. Tluchoř, *Nuclear Fusion* **31**, 711 (1991).
- [13] A. K. Ram, J. Decker, and Y. Peysson, *J. Plas. Phys.* **71**, 675 (2005).
- [14] E. Poli, *Fusion Science and Technology* **53**, 1 (2008).
- [15] M. Bornatici *et al.*, *Nuclear Fusion* **23**, 1153 (1983).
- [16] P. T. Bonoli, and R. C. Englade, *Physics of Fluids* **29**, 2937 (1986).
- [17] N. B. Marushchenko, H. Maassberg, and Y. Turkin, *Nuclear Fusion* **48**, 054002 (2008).
- [18] F. R. Hansen *et al.*, *J. Plas. Phys.* **39**, 319 (1988).
- [19] R. H. Cohen, *Physics of Fluids* **30**, 2442 (1987).
- [20] J. Decker, A. K. Ram, and Y. Peysson, in *17th Topical Conference on Radio Frequency Power in Plasmas* (Clearwater, Florida, USA, 2007).
- [21] M. Ono *et al.*, *Nuclear Fusion* **40**, 557 (2000).
- [22] B. Lloyd *et al.*, *Nuclear Fusion* **47**, S658 (2007).
- [23] J. Preinhaelter *et al.*, in *16th Topical Conference on Radio Frequency Power in Plasmas*, edited by J. W. Stephen, and T. B. Paul (AIP, Park City, Utah, USA, 2005), pp. 349.
- [24] J. Urban *et al.*, in *33rd Annual European Physical Society Conference on Controlled Fusion and Plasma Physics*, edited by F. D. Marco, and G. Vlad (EPS, Roma, Italy, 2006), pp. P5.171.
- [25] J. Urban *et al.*, in *14th Joint Workshop on Electron Cyclotron Emission and Electron Cyclotron Resonance Heating*, edited by A. Lazaros (Heliotospos Conferences Ltd., Santorini, Greece, 2006), pp. 194.
- [26] S. J. Diem *et al.*, in *49th Annual Meeting of the Division of Plasma Physics*, edited by G. Sprouse (APS, Orlando, FL, USA, 2007), p. 63.
- [27] Y. Y. Podoba *et al.*, *Physical Review Letters* **98**, 255003 (2007).
- [28] S. P. Hirshman, and W. I. Vanrij, *Computer Physics Communications* **43**, 143 (1986).
- [29] J. Preinhaelter *et al.*, in *17th Topical Conference on Radio Frequency Power in Plasmas*, edited by P. M. Ryan, and D. Rasmussen (AIP, Clearwater, FL, USA, 2007), pp. 343.
- [30] H. P. Laqua *et al.*, in *49th Annual Meeting of the Division of Plasma Physics*, edited by G. Sprouse (APS, Orlando, FL, USA, 2007), pp. 280.
- [31] J. Preinhaelter *et al.*, in *35th EPS Plasma Physics Conference* (EPS, Hersonissos, Crete, Greece, 2008).